IEEE Photonics Journal
An IEEE Photonics Society Publication

Open Access

A Stopband and Passband Switchable Microwave Photonic Filter Based on Integrated Dual Ring Coupled Mach–Zehnder Interferometer

Volume 11, Number 4, August 2019

Huimin Yang
Jing Li
Pengfei Zheng
Guohua Hu
Binfeng Yun
Yiping Cui

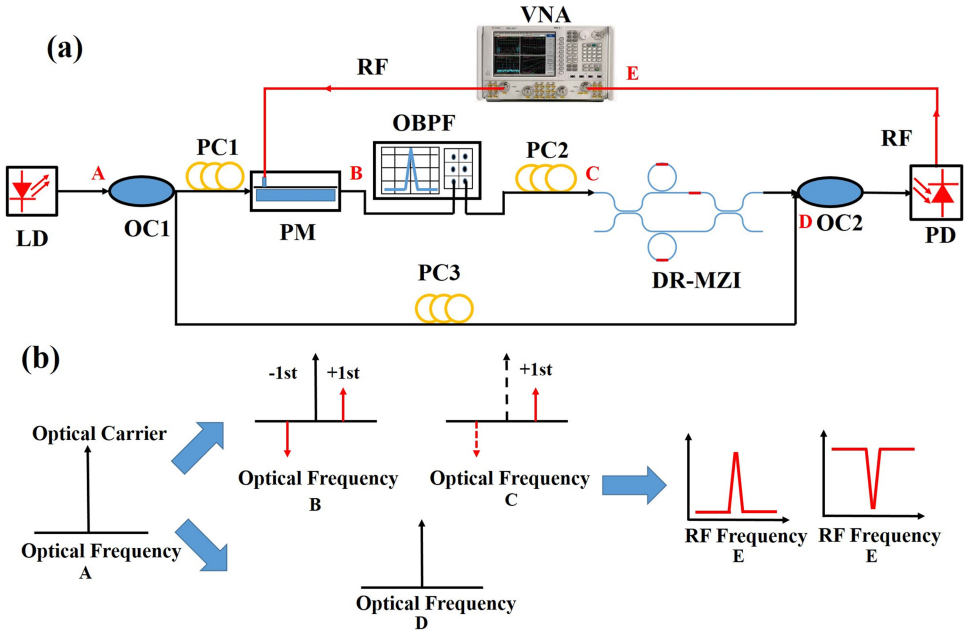

DOI: 10.1109/JPHOT.2019.2928834
1943-0655

A Stopband and Passband Switchable Microwave Photonic Filter Based on Integrated Dual Ring Coupled Mach–Zehnder Interferometer

Huimin Yang, Jing Li, Pengfei Zheng, Guohua Hu, Binfeng Yun, and Yiping Cui

Advanced Photonics Center, Southeast University, Nanjing 210096, China

DOI:10.1109/JPHOT.2019.2928834

Manuscript received June 24, 2019; accepted July 11, 2019. Date of publication July 19, 2019; date of current version August 1, 2019. This work was supported in part by the National Key R&D Program of China under Grant 2018YFB2201800, in part by the National Science Foundation of China under Grants 61535003 and 61601118, and in part by the National Science Foundation of Jiangsu Province under Grant BK 20161429. Corresponding authors: Binfeng Yun; Yiping Cui (email: ybf@seu.edu.cn; cyp@seu.edu.cn).

Abstract: A stopband and passband switchable microwave photonic filter based on the integrated tunable dual ring coupled Mach–Zehnder interferometer has been demonstrated. By using the optical single sideband modulation, the switchable stopband and passband optical responses of the optical filter are one-to-one mapping to the RF spectra. The center frequency and bandwidth of the switchable microwave photonic filter are both reconfigurable. A frequency tuning range of 4–25 GHz is obtained, and the bandwidth tuning ranges of the passband and stopband MPFs are 4.54–9.72 GHz and 3.65–6.35 GHz, respectively. In addition, a RF rejection ratio about 20 dB is achieved. Compared with the switchable MPFs implemented by nonintegrated devices, the proposed switchable MPF provides a simple and low cost method to process radiofrequency signals.

Index Terms: Microwave photonic filter, microring resonator, Mach-Zehnder interferometer, silicon nitride.

1. Introduction

Microwave photonic (MWP) technology can achieve the purpose of processing radiofrequency (RF) signals in optical domain with its intrinsic advantages of low loss, large bandwidth, reconfigurability and immunity to electromagnetic interferences [1], [2]. As an important building block of MWP technology, microwave photonic filters (MPFs) have attracted a lot of research interests in RF signals processing [1]–[21] and have been widely applied in the field of wireless communications, radar, beamforming and radio astronomy [3], [4]. To date, MPFs based on fiber components such as Fabry-Perot filter [5]–[7], fiber Bragg grating [8], [9] and stimulated Brillouin scattering (SBS) [10]–[12] have been reported. However, these MPFs based on the bulky fiber components are relative unstable and lack of reconfigurability [8]. In order to overcome these shortcomings, integrated MPFs with much more compact size and better tenability have attracted researchers' attention. Until now, integrated MPFs based on integrated optical filters such as micro-ring resonator (MRR) [13]–[17], Mach-Zehnder interferometer (MZI) [18], [19], micro disk resonator [20] and so on have

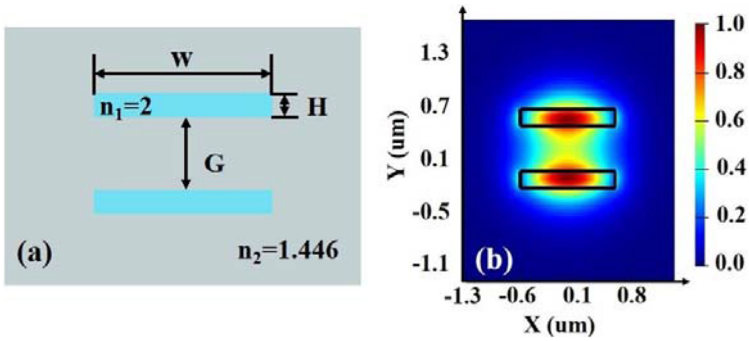

Fig. 1. (a) The waveguide cross-section of the double strip Si_3N_4 waveguide. (b) $|E|^2$ distribution of the fundamental TE mode.

been reported. Among them, a notch MPF was achieved by using optical single sideband (OSSB) modulation and an optical notch filter, frequency tuning range of 2∼8 GHz and out of band RF rejection of more than 60 dB were achieved [13]. In Ref [16], a bandpass MPF was achieved by using phase modulation (PM) and an optical notch filter, whose frequency can be tuned from 2 to 18.4 GHz, the obtained bandwidth and out of band RF rejection are 170 MHz and 26.5 dB, respectively. A bandpass MPF was achieved by using intensity modulation (IM) and an optical bandpass filter [18], the filter's frequency and bandwidth tuning range are 18∼40 GHz and 5∼15 GHz, respectively. In these schemes, the filter's frequency and bandwidth can be reconfigured, but only bandpass or bandstop MPF can be realized. In Ref [21], a bandpass and bandstop switchable MPF was achieved by using PM and two tunable optical bandpass filters (TOBF). However, the proposed switchable MPF is based on discrete optical devices, which make the system bulky and complex. Besides, the filter's frequency and bandwidth can not be easily tuned due to the limitations of TOBF [21]. In order to achieve an integrated bandpass and bandstop switchable MPF with reconfigurable frequency and bandwidth, here we propose a MPF by using PM and integrated dual-ring coupled Mach-Zehnder interferometer (DR-MZI). By switching the response of the DR-MZI filter, a bandpass and bandstop switchable MPF was achieved with OSSB modulation, which realized the one-to-one mapping from optical response to RF response [22], [23]. For the bandpass MPF, a filter frequency tuning range of 4 GHz∼25 GHz and bandwidth tuning range of 4.54 GHz∼9.72 GHz were achieved. And for the notch MPF, the filter's frequency and bandwidth can be tuned from 4 GHz∼25 GHz and 3.65 GHz∼6.35 GHz, respectively. In addition, the RF rejection ratio about 20 dB is achieved.

2. Filter Structure

The proposed tunable optical filter based on DR-MZI is fabricated by the double stripe silicon nitride waveguide platform (TriPleX^{TM}) [24]. The cross-section of the double stripe silicon nitride waveguide is shown in Fig. 1(a), where two silicon nitride stripes with thickness of H = 0.17 μm as waveguide core are embedded in silica. The waveguide width is W = 1.2 μm, and the gap size between the two silicon nitride stripes is G = 0.5 μm. Here the fundamental TE mode is used and its mode profile is shown in Fig. 1(b).

Fig. 2 shows the schematic of the proposed tunable optical filter based on DR-MZI. Two tunable MRRs with the same perimeter of 2.927 mm are coupled to the two arms of MZI. The coupling gap between MRR and the MZI is 1 μm. Combined with the waveguide's group index of 1.71, a free spectral region (FSR) of about 60 GHz for the MRR is obtained. Because the MZI is symmetrical, the FSR of the DR-MZI is determined by the MRR. Three phase shifters are achieved by using thermo-optic heaters on the MRRs and the top arm of MZI, respectively.

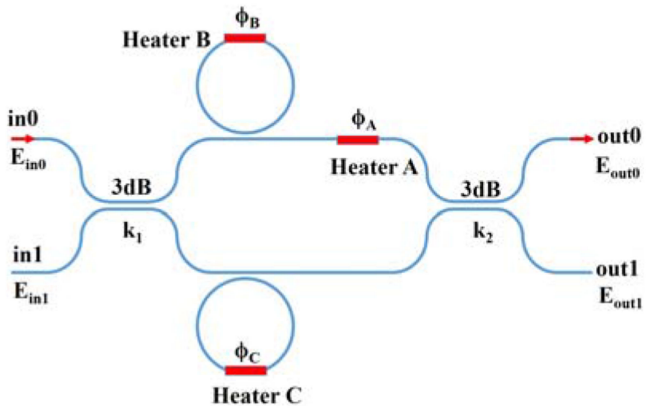

Fig. 2. The schematic of the tunable DR-MZI filter.

The optical response of the tunable DR-MZI filter can be modeled by using the transfer matrix method, which can be written as follows:

$$\begin{bmatrix} E_{out0} \\ E_{out1} \end{bmatrix} = \begin{bmatrix} \sqrt{1-k_2} & -i\sqrt{k_2} \\ -i\sqrt{k_2} & \sqrt{1-k_2} \end{bmatrix} \begin{bmatrix} e^{-j\phi_A} H_1 & 0 \\ 0 & H_2 \end{bmatrix} \begin{bmatrix} \sqrt{1-k_1} & -i\sqrt{k_1} \\ -i\sqrt{k_1} & \sqrt{1-k_1} \end{bmatrix} \begin{bmatrix} E_{in0} \\ E_{in1} \end{bmatrix} \quad (1)$$

Where ϕ_A represents the additional phase induced by the heater A. k_1 and k_2 are the power coupling coefficients of the two 3 dB directional couplers (DC). E_{in0} and E_{in1} represent the input electric fields, E_{out0} and E_{out1} represent the output electric fields. H_1 and H_2 represent the transfer function of the two MRRs, which can be written as follows:

$$H_n(\varphi) = \frac{t - ae^{-i(\phi+\varphi)}}{1 - tae^{-i(\phi+\varphi)}} (n = 1 \text{ or } 2) \quad (2)$$

where t represents the amplitude coupling coefficient of the MRR, a represents the round-trip loss factor. When $a = 1$, it means that the MRR is lossless. ϕ represents the additional phases induced by heater B or C on the MRRs, φ represents the phase shift of the light propagating in the MRR. And the optical response of the DR-MZI can be obtained by combining Eq. (1) and Eq. (2).

As shown in Fig. 2, the output of the proposed DR-MZI is based on the interferences between the top and bottom optical branches in the balanced MZI. Assume the optical phases of top and bottom optical paths in the MZI are φ_u and φ_L , respectively. Here the light is input from in0, the optical output at out0 should be determined by the phase difference between top and bottom optical paths, which is $\Delta\varphi = \varphi_u - \varphi_L$. For switching between the stopband and passband filter, we just need to change $\Delta\varphi$ by altering the additional phase shift using the heater A, while the additional phase difference caused by the two MRRs at resonance is fixed. We simulated the phase difference $\Delta\varphi$ between top and bottom optical paths of the stopband and passband filters and the results are shown in Fig. 3. When $\Delta\varphi$ is adjusted to about π at filter's resonant wavelength as shown in Fig. 3(a), destructive interference occurs and the stopband filter can be obtained. On the contrary, the passband filter can be obtained when $\Delta\varphi$ is adjusted to about 0 at resonant wavelength as shown in Fig. 3(b), where constructive interference occurs.

3. Experimental Results and Discussion

First, by inputting tunable laser from in0 port and detecting at out0 port, the optical spectra of the proposed unable DR-MZI filter was measured using the Agilent lightwave measurement system (81640A). By adjusting the voltages applied on the heaters on the MRRs and the top arm of MZI, the bandpass and bandstop spectra of the optical filter were measured. Assuming V_A, V_B, and V_C

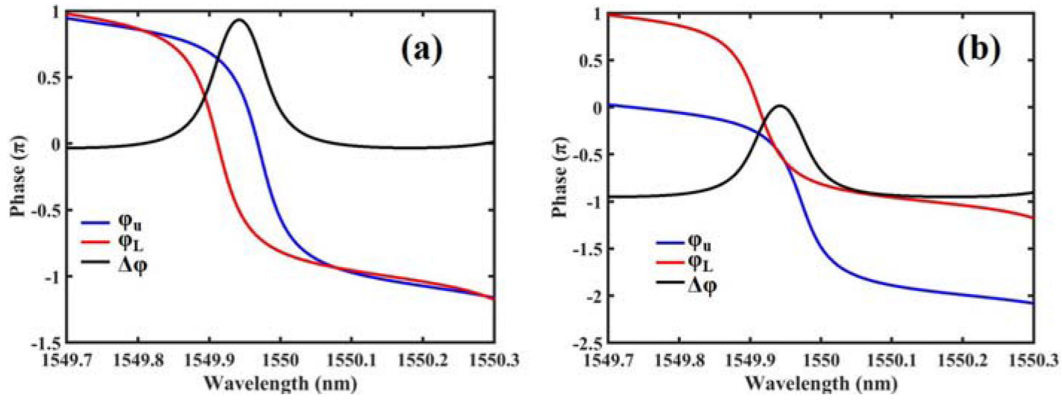

Fig. 3. The phase of (a) a stopband filter and (b) a passband filter.

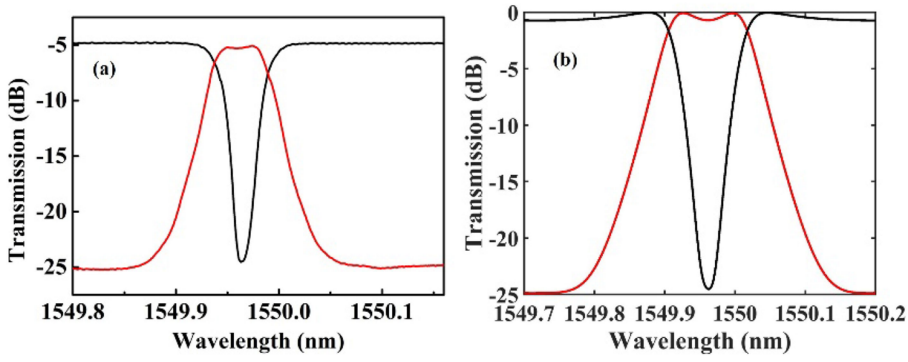

Fig. 4. The (a) measured and (b) simulated transmission spectra of the switchable DR-MZI filter.

represent the voltages of heater A, B and C, respectively. When voltage combination of $V_A = 7.2$ V, $V_B = 4$ V and $V_C = 6.45$ V are chosen, a bandpass optical filter is obtained. While when $V_A = 15.6$ V, $V_B = 0$ V and $V_C = 5.2$ V are applied, a bandstop optical filter is realized. The measured transmission spectra of the optical filter are shown in Fig. 4(a). Also the corresponding theoretical spectra were simulated and shown in Fig. 4(b) with $a = 0.9961$, $t = 0.6739$, $k_1 = 0.4714$ and $k_2 = 0.5285$, which are obtained by fitting the measured bandstop spectrum using Eq. (1) and Eq. (2). Because the round-trip loss factor is larger than the amplitude coupling coefficient of the MRR ($a > t$), so the two MRRs are both over coupled. It can be seen that the experimental results are in good agreement with the simulation results. And as can be seen in Fig. 4(a), extinction ratios (ER) of about 20 dB are measured for both the optical bandpass and bandstop responses, and 3 dB bandwidths are about 6 GHz and 7 GHz for the optical bandstop and bandpass filters, respectively.

By using the optical DR-MZI filter, the proposed stopband and passband switchable MPF were realized by using the experimental setup shown in Fig. 5. The optical carrier signal emitted by the laser diode (LD, Santac WSL-100) is divided into two parts by the 3 dB optical coupler (OC1), one part of the optical carrier is modulated by a phase modulator (Eospace, PM-0S5-20-PFA-PFA), while the other part of the optical carrier is not modulated. When the optical carrier is modulated by RF signal from vector network analyzer (VNA, Agilent, N5242A), optical double sideband modulation (ODSB) can be realized and $+1$st and -1st order optical sideband signals with π phase difference can be obtained. A tunable optical bandpass filter (OBPF) is used to filter the optical carrier and the -1st order optical sideband signal.

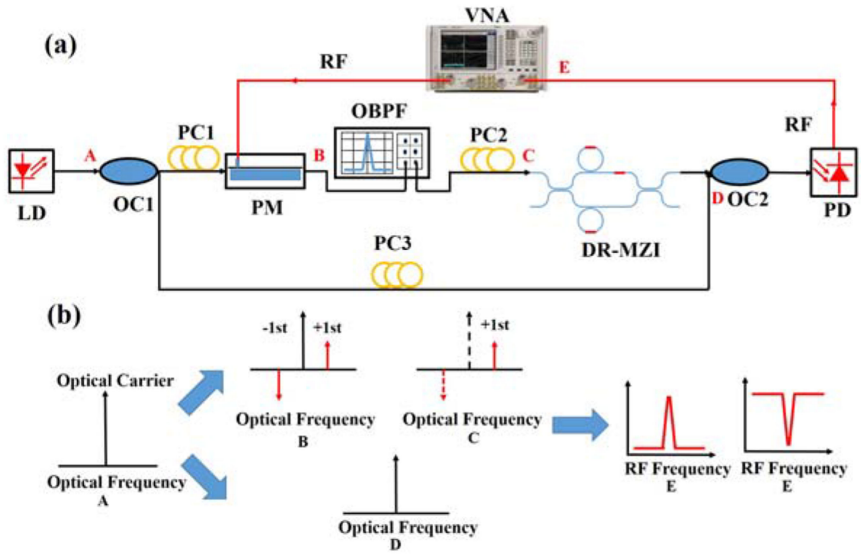

Fig. 5. (a) The scheme of the proposed switchable MPF. (b) The principle diagram of the proposed switchable MPF in frequency domain.

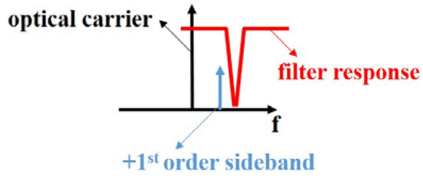

Fig. 6. The schematic diagram of single sideband principle.

As shown in Fig. 6, when the optical carrier is fixed at the low frequency side of the filter's resonance, the remained +1st order optical sideband is scanned one-to-one in the frequency region from low to high frequency.

When the unmodulated optical carrier and the +1st order optical sideband are combined through the OC2 and then applied to a high speed photodetector (PD, Finisar XPDV2120RA), the beating between the unmodulated optical carrier and the +1st order optical sideband will generate a photocurrent which can be written as follow:

$$\begin{aligned} \mathrm{i} &= \eta \mathrm{E}_{\mathrm{out}} \mathrm{E}_{\mathrm{out}}^{*} = \alpha\eta \mathrm{P}_{\mathrm{c}} \mathrm{H}(\omega_0 + \omega_{\mathrm{f}}) \mathrm{e}^{\mathrm{j}\omega_{\mathrm{f}}\mathrm{t}} \\ \mathrm{E}_{\mathrm{out}} &= E_0 + E_{+1} \\ &= \frac{\sqrt{2}}{2} \mathrm{E}_{\mathrm{c}} \mathrm{e}^{\mathrm{j}(\omega_0+\varphi_0)} + \frac{\sqrt{2}}{2} \mathrm{E}_{\mathrm{c}} \mathrm{e}^{\mathrm{j}\varphi_0} \mathrm{J}_1(\mathrm{m}) \mathrm{e}^{\mathrm{j}(\omega_0+\omega_{\mathrm{f}})\mathrm{t}} \mathrm{H}(\omega_0 + \omega_{\mathrm{f}}) \end{aligned} \tag{3}$$

Where α is the loss of the link, η is the responsivity of PD, P_c is light power. And α, η and P_c can be regarded as contains. E_0 and E_{+1} represent the electric fields of optical carrier and +1st order optical sideband, respectively. E_c is electric field of input optical carrier, ω_0 is the angular frequency of optical carrier, ω_f is the angular frequency of RF signal, φ_0 is the phase of optical carrier. *J(m)* is Bessel function of the first kind, $H(\omega)$ is the amplitude transfer function of optical filter. So the output

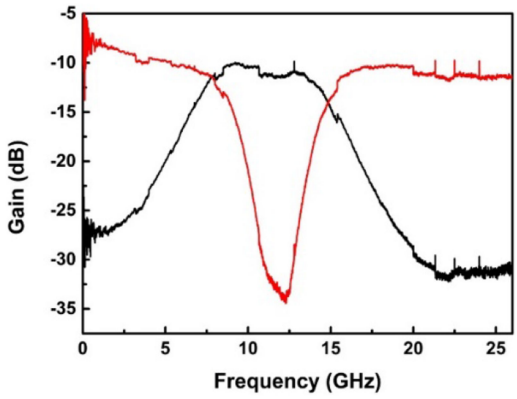

Fig. 7. The measured switchable bandpass and bandstop spectra of the MPF.

RF power P_{out} can be written as follow:

$$\begin{aligned} P_{out} &= \frac{1}{2}\langle i\rangle^2 R_{out} \\ &= \frac{1}{2}\left[\frac{\alpha\eta P_c\,|H(\omega_0+\omega_f)|}{\sqrt{2}}\right]^2 R_{out} \\ &= \frac{1}{4}\alpha^2\eta^2 P_c^2 R_{out} T(\omega_0+\omega_f) \end{aligned} \tag{4}$$

Where R_{out} is the matched impedance, and $T(\omega_0+\omega_f) = |H(\omega_0+\omega_f)|^2$ is the optical transmission function of the DR-MZI. According to Eq. (4), the obtained RF power P_{out} is proportional to $T(\omega_0+\omega_f)$, which is the optical transmission function of the DR-MZI optical filter. So the optical transmission spectrum of the proposed DR-MZI filter can be one-to-one mapping to the RF power spectrum. The polarization controllers (PC1, PC2 and PC3) were adjusted in order to reduce the optical loss. Using this MWP link, the bandpass and bandstop response of the optical DR-MZI filter can be mapped to the microwave domain. In addition, the frequency of the proposed MPF can be tuned by changing the wavelength difference between the optical carrier and the optical filter, and the reconfigurable bandwidth of the proposed MPF can be achieved by varying the optical DR-MZI filter's bandwidth, which can be achieved by changing V_C.

As the optical filters, when the heater voltage combinations of $V_A = 7.2$ V, $V_B = 4$ V and $V_C = 6.45$ V are changed to $V_A = 15.6$ V, $V_B = 0$ V and $V_C = 5.2$ V, the RF responses of the MPF are changed from bandpass to bandstop, which are shown in Fig. 7. It can be seen that the center frequency of the MPF is about 12 GHz and the RF rejection ratios are about 20 dB and 25 dB for the bandpass to bandstop responses.

The center frequency and 3 dB bandwidth of the switchable MPF can also be tuned for the bandpass response and the results are shown in Fig. 8. The center frequency of the bandpass MPF can be changed by varying the wavelength of the optical carrier. Theoretically, the frequency tuning range of the MPF can reach 30 GHz because the FSR of the optical filter is 60 GHz. However due to the limited frequency range of the VNA (0-26.5 GHz), only the frequency tuning range of 4 GHz$\sim$25 GHz are measured and shown in Fig. 8(a). On the other hand, the bandwidth of the bandpass MPF can be reconfigured by changing V_C and the results are shown in Fig. 8(b). From Fig. 8(b), it can be seen that when V_C is varied from 4.6 V to 5.8 V, the bandwidth of the bandpass MPF can be changed from 4.54 GHz to 9.72 GHz. And flat passbands with out-of-band RF rejection ratio about 20 dB and less than 1.3 dB in band fluctuation were obtained.

Also the bandstop spectra of the switchable MPF were measured as shown in Fig. 9(a). The measured frequency tuning range of the bandstop MPF is 4 GHz$\sim$25 GHz. By changing V_C from

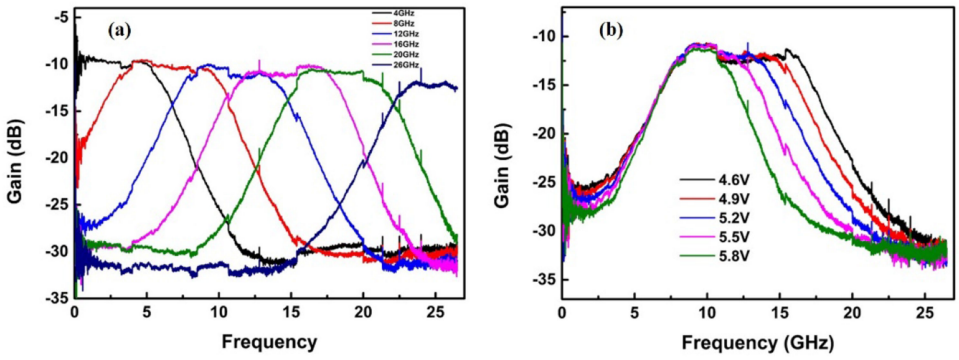

Fig. 8. The (a) frequency and (b) bandwidth reconfigurabilities of the bandpass MPF's responses.

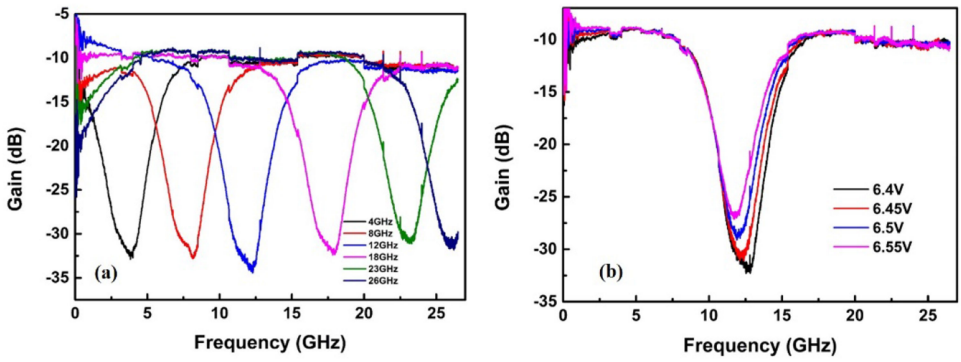

Fig. 9. The (a) frequency and (b) bandwidth reconfigurabilities of the bandstop MPF's responses.

6.4 V∼6.55 V, the bandwidth of the bandstop MPF can be reconfigurable from 3.65 GHz∼6.35 GHz as shown in Fig. 9(b).

In addition, here we have to separate the optical carrier and selected single sideband via two optical fiber branches in order to realize the passband and stopband microwave photonic filters with same microwave photonic link, otherwise the optical carrier will be suppressed and no passband microwave photonic filter response can be obtained because the optical carrier should be placed outside of the resonance band of the DR-MZI filter. However, the optical phase difference between the two fiber branches can be changed by environmental fluctuations, which will change the phase response of the proposed MPF. However, the amplitude response of the MPF will not be affected by this phase difference variation as long as the optical carrier and −1st order sideband are well filtered by the tunable optical passband filter. So a tunable optical passband filter with steep edge is preferred. And in order to get a stable phase response of the MPF, possible solution is to integrate the whole system into a single chip with temperature stabilized packaging.

4. Conclusion

In conclusion, the passband and stopband switchable MPF were achieved by switching the responses of the optical filter consisting of dual-ring assisted MZI, which were achieved by changing the voltages of heaters on the MRRs and the top arm of MZI. Due to the OSSB modulation, the responses of the optical filter can be one-to-one mapped to the responses of the MPF, so the switchable MPF can be realized. In addition, the switchable MPF is also tunable and reconfigurable, the frequency tuning range is 4 GHz∼25 GHz for the bandpass and the bandstop responses, and the bandwidth reconfigurable ranges are 4.54 GHz∼9.72 GHz for the passband MPF and

3.65 GHz∼6.35 GHz for the stopband MPF, respectively. And by using a dual-parallel Mach-Zehnder modulator (IQ modulator) to produce optical carrier suppressed singles sideband modulation, the proposed switchable MPF has the potential to be full integrated in a chip with hybrid integrated technologies and could be widely used in microwave photonic signal processing systems.

References

[1] M. P. Fok and J. Ge, "Tunable multiband microwave photonic filters," *Photonics*, vol. 4, no. 4, 2017, Art. no. 45.
[2] J. Capmany and D. Novak, "Microwave photonics combines two worlds," *Nature Photon.*, vol. 1, no. 6, pp. 319–330, 2007.
[3] B. Yu *et al.*, "Silica-microsphere-cavity-based microwave photonic notch filter with ultra-narrow bandwidth and high peak rejection," *Opt. Lett.*, vol. 44, no. 6, pp. 1411–1414, 2019.
[4] R. Maram, S. Kaushal, J. Azaña, and L. R. Chen, "Recent trends and advances of silicon-based, integrated microwave photonics," *Photonics*, vol. 6, no. 1, 2019, Art. no. 13.
[5] J. Wo *et al.*, "Fibre axial strain sensor based on a microwave photonic filter with dualpassband,"*J. Mod. Opt.*, vol. 65, no. 14, pp. 1737–1741, 2018.
[6] F. Jiang, Y. Yu, T. Cao, H. Tang, J. Dong, and X. Zhang, "Flat-top bandpass microwave photonic filter with tunable bandwidth and center frequency based on a Fabry–Pérot semiconductor optical amplifier," *Opt. Lett.*, vol. 41, no. 14, pp. 3301–3304, 2016.
[7] F. Jiang, Y. Yu, H. Tang, Lu Xu, and X. Zhang, "Tunable bandpass microwave photonic filter with ultrahigh stopband attenuation and skirt selectivity," *Opt. Exp.*, vol. 24, no. 16, pp. 18655–18663, 2016.
[8] N. Shi, T. Hao, W. Li, N. Zhu, and M. Li, "A reconfigurable microwave photonic filter with flexible tunability using a multi-wavelength laser and a multi-channel phase-shifted fiber Bragg grating," *Opt. Commun.*, vol. 407, pp. 27–32, 2018.
[9] E. Xu, S. Pan, Z. Zhang, and P. Li, "Performance-improved microwave photonic single-passband filter using birefringence of phase-shifted fiber Bragg grating," *Opt. Commun.*, vol. 428, pp. 41–46, 2018.
[10] D. Samaniego and B. Vidal, "Brillouin microwave filter with enhanced skirt selectivity using a birefringent fiber," *IEEE Photon. Technol. Lett.*, vol. 31, no. 6, pp. 431–434, Mar. 2019.
[11] Z. Li *et al.*, "Tunable dual-passband microwave photonic filter with a fixed frequency interval using phase-to-intensity modulation conversion by stimulated Brillouin scattering," *Appl. Opt.*, vol. 58, no. 8, pp. 1961–1965, 2019.
[12] J. Yan, L. Li, X. Yi, and S. X. Chew, "Widely tunable single bandpass microwave photonic filter based on dual-fiber stimulated Brillouin scattering," *Microw. Opt. Technol. Lett.*, vol. 61, no. 4, pp. 954–958, 2019.
[13] D. Marpaung *et al.*, "Si3N4 ring resonator-based microwave photonic notch filter with an ultrahigh peak rejection," *Opt. Exp.*, vol. 21, no. 20, pp. 23286–23294, 2013.
[14] C. Taddei, L. Zhuang, C. G. H. Roeloffzen, M. Hoekman, and K.-J. Boller, "High-selectivity on-chip optical bandpass filter with sub-100-MHz flat-top and under-2 shape factor," *IEEE Photon. Technol. Lett.*, vol. 31, no. 6, pp. 455–458, Mar. 2019.
[15] Z. Zhang, B. Huang, Z. Zhang, C. Cheng, and H. Chen, "Microwave photonic filter with reconfigurable and tunable bandpass response using integrated optical signal processor based on microring resonator," *Opt. Eng.*, vol. 52, no. 12, pp. 1–7, 2013.
[16] H. Qiu *et al.*, "A continuously tunable sub-gigahertz microwave photonic bandpass filter based on an ultra-high-Q silicon microring resonator," *J. Lightw. Technol.*, vol. 36, no. 19, pp. 4312–4318, Oct. 2018.
[17] S. Song, S. X. Chew, X. Yi, L. Nguyen, and R. A. Minasian, "Tunable single passband microwave photonic filter based on integrated optical double notch filter," *J. Lightw. Technol.*, vol. 36, no. 19, pp. 4557–4564, Oct. 2018.
[18] D. Zhang, X. Feng, and Y. Huang, "Tunable and reconfigurable bandpass microwave photonic filters utilizing integrated optical processor on silicon-on-insulator substrate," *IEEE Photon. Technol. Lett.*, vol. 24, no. 17, pp. 1502–1505, Sep. 2012.
[19] Q. Sun, L. Zhou, L. Lu, G. Zhou, and J. Chen, "Reconfigurable high-resolution microwave photonic filter based on dual-ring-assisted MZIs on the Si_3N_4 platform," *IEEE Photon. J.*, vol. 10, no. 6, Dec. 2018, Art. no. 6602612.
[20] W. Zhang and J. Yao, "Integrated frequency-tunable microwave photonic bandpass filter on a silicon photonic chip," *Opt. Lett.*, vol. 43, no. 15, pp. 3622–3625, 2018.
[21] Y. Yu, E. Xu, J. Dong, L. Zhou, X. Li, and X. Zhang, "Switchable microwave photonic filter between high Q bandpass filter and notch filter with flat passband based on phase modulation," *Opt. Express.*, vol. 18, no. 24, pp. 25271–25282, 2010.
[22] J. S. Fandifio, P. Muñoz, D. Doménech, and J. Capmany, "A monolithic integrated photonic microwave filter," *Nature Photon.*, vol. 11, no. 1, pp. 124–130, 2016.
[23] X. Liu, Y. Yu, H. Tang, L. Xu, J. Dong, and X. Zhang, "Silicon-on-insulator-based microwave photonic filter with narrowband and ultrahigh peak rejection," *Opt. Lett.*, vol. 43, no. 6, pp. 1359–1362, 2018.
[24] W. Hoving, R. Heideman, D. Geuzebroek, A. Leinse, E. Klein, and R. Dekkera, "Low loss, high contrast planar optical waveguides based on low-cost CMOS compatible LPCVD processing," *Proc. SPIE*, vol. 6996, 2008, Art. no. 699612.